Quantum chemistry calculations for molecules coupled to reservoirs: Formalism, implementation, and application to benzenedithiol

Cite as: J. Chem. Phys. **126**, 174101 (2007); https://doi.org/10.1063/1.2716664
Submitted: 15 November 2006 . Accepted: 21 February 2007 . Published Online: 01 May 2007

A. Arnold, F. Weigend, and F. Evers

Quantum chemistry calculations for molecules coupled to reservoirs: Formalism, implementation, and application to benzenedithiol

A. Arnold
Institut für Theorie der kondensierten Materie, Universität Karlsruhe, 76128 Karlsruhe, Germany

F. Weigend
Institut für Nanotechnologie, Forschungszentrum Karlsruhe, 76021 Karlsruhe, Germany

F. Evers
Institut für Theorie der kondensierten Materie, Universität Karlsruhe, 76128 Karlsruhe, Germany and
Institut für Nanotechnologie, Forschungszentrum Karlsruhe, 76021 Karlsruhe, Germany

(Received 15 November 2006; accepted 21 February 2007; published online 1 May 2007)

Modern quantum chemistry calculations are usually implemented for isolated systems—big molecules or atom clusters; total energy and particle number are fixed. However, in many situations, like quantum transport calculations or molecules in a electrochemical environment, the molecule can exchange particles (and energy) with a reservoir. Calculations for such cases require to switch from the canonical to a grand canonical description, where one fixes the chemical potential rather than particle number. To achieve this goal, the authors propose an implementation in standard quantum chemistry packages. An application to the nonlinear charge transport through 1,4-benzenedithiol will be presented. They explain the leading finite bias effect on the transmission as a consequence of a nonequilibrium Stark effect and discuss the relation to earlier work. © *2007 American Institute of Physics*. [DOI: 10.1063/1.2716664]

I. INTRODUCTION

Many charge transfer processes can be described using the concept of *partitioning*. One identifies an atomistic subsystem and refers to the remaining degrees of freedom of the entire system as the "reservoir." Partitioning is very useful, if it is justified to use crude approximations for the theoretical treatment of the reservoirs without losing any accuracy in the calculation of the subsystem observables of interest.

To be specific, we focus on the example of charge transport through individual molecules. Then, the atomistic subsystem of our concern is the molecule (and perhaps a very small part of the leads); two reservoirs model the left and the right hand side electrodes. We emphasize, however, that the fundamental concepts explicated here would equally well apply to many other problems of interest as well, e.g., molecules in an electrolyte environment.

Some standard quantum chemistry codes, such as TURBOMOLE,[1] are optimized for *ab initio* calculations of large molecular systems. This would make them particularly attractive for molecular transport studies. However, such codes do not provide internal degrees of freedom that could accomodate an exchange of particles and thus model a reservoir. Instead, they are typically designed to work inside a trivial vacuum with a dielectric constant of unity, $\epsilon_0=1$. Admittedly, exceptions are available, where the vacuum is replaced by a conductor like screening model[2] simulating an environment characterized by a dielectric constant $\epsilon_0 \neq 1$. This is implemented by a change in the boundary condition when solving the Schrödinger equation; for a metallic environment, for instance, it is given by a (equipotential) surface surrounding the molecule or atomic cluster. Nevertheless, also in these cases exchange of particles with the environment is usually not permitted.

With respect to this exchange of particles, codes optimized for band structure calculations are in a better shape, because employing periodic boundary conditions, a reservoir is automatically included; effectively, one works at constant μ rather than constant particle number N (in the sense that the electron number per unit cell adjusts itself according to the requirements of charge neutrality). However, with these codes, the molecules that we would like to deal with, can be treated only at the price of introducing very large unit cells ("slab method")—too large for many practical purposes.

We present here a method to include reservoirs in a quantum chemical approach. A brief outline of the proposed procedure is as follows: since particles can leave the subsystem and disappear in the thermodynamic bath, time evolution is no longer unitary; the energy levels experience lifetime broadening. In technical terms, the resolvent operator $\mathcal{G}$ describing the subspace dynamics (time evolution operator for dynamics of electrons on the molecule) has the structure

$$\mathcal{G}^{-1} = \mathcal{G}_0^{-1} - \Sigma. \tag{1}$$

$\mathcal{G}_0$ describes the uncoupled system. As usual, all operators can be thought of as matrices (e.g., for noninteracting particles: $\langle x|\mathcal{G}_0|x'\rangle = \langle x|e^{-iH_0(t-t')}|x'\rangle$, with $x=(\mathbf{x},t)$, and H_0 describing the uncoupled system). The self-energy Σ incorporates the non-Hermitian pieces, which transform the unitary time evolution of the uncoupled system, $\mathcal{G}_0$, into the nonunitary evolution of $\mathcal{G}$.

Equation (1) is trivially exact and always valid, since it is merely a definition of Σ. The difficulty arises when Σ is to

be calculated for a definite problem at hand. Only at this point the various different physical realizations of the reservoir(s) (and other damping mechanisms) differ from each other.

The approach that we propose here assumes that Σ is given. It is most useful in the situation when Σ can be modeled as a matrix with an arbitrary spatial structure, but diagonal in time (i.e., a constant in energy representation). The validity of this approximation makes partitioning a good concept.

In practical terms, the nonunitary time evolution, Eq. (1), affects the iteration cycles underlying the self-consistent single particle theories of quantum chemistry and electronic structure codes. Crucially, intrusion occurs only at a single step, namely, when the density operator is calculated. In the presence of Σ an expression originating from the nonequilibrium Green's function formalism [see Eq. (4) below] has to be employed rather than the slightly simpler one derived for isolated systems [Eq. (8)].

Our formalism has already been applied successfully and tested against experiments for calculations of charge transport properties of individual molecules.[3–5] A detailed explication of the method's variant appropriate for this nonequilibrium problem is offered below. Let us stress, however, that the scope of possible applications of the procedure is much broader than this. In order to illustrate the general perspectives more clearly, emphasis of the presentation shall be on the salient physical aspects of the procedure rather than technical derivations. For the latter, we refer the reader to the standard literature.[6,7]

II. METHOD

Quantum chemistry calculations can be equipped with reservoirs by modifying the Schrödinger dynamics of the isolated system with Eq. (1). For self-consistent single particle theories, such as Hartree-Fock or density functional theory (DFT), the procedure is straightforward and will be explained now.

A. Self-consistency cycle

A standard self-consistency cycle can be understood to consist of two essential steps. In the first step, the effective single particle Hamiltonian, $H[n,j]$, is calculated. In general, it may depend on particle $n(\mathbf{x})$ and current densities $j(\mathbf{x})$, i.e., H is a functional of the density operator. In the second step, H is used in order to construct an update of the density matrix. This update is a crucial step. Here the boundary conditions enter that regulate how eigenstates of $H[n,j]$ are to be filled up in order to obtain the particle density, current, etc. Rules differ, depending on whether, e.g., an interface to free vacuum, to an electrode, or an electrochemical environment is to be modeled.

The procedure of calculating the density matrix is most transparent when formulated with a "Keldysh" Green's function

$$\mathcal{G}^{<} = \mathcal{G}\Sigma^{<}\mathcal{G}^{\dagger}, \tag{2}$$

where

$$\mathcal{G}^{-1}(E) = E - H - \Sigma. \tag{3}$$

$\mathcal{G}^{<}$ relates to the density matrix via

$$n(\mathbf{x},\mathbf{x}') = \frac{i}{\pi}\int dE\langle \mathbf{x}|\mathcal{G}^{<}(E)|\mathbf{x}'\rangle. \tag{4}$$

The Keldysh object $\Sigma^{<}$ incorporates the effects of any thermodynamic bath (different interfaces but also phonons, vibrons, photons, etc.) that the molecule can couple to. It is described in the following two sections. Equipped with a proper expression for $\Sigma^{<}$, this last equation, Eq. (4), is used in order to recalculate $n(\mathbf{x},\mathbf{x}')$ and then $H[n,j]$ for the next iteration.

B. Keldysh formalism for noninteracting particles

At this point, we refer to standard monographs for a general background on the nonequilibrium Green's function (Keldysh) formalism and for rigorous derivations.[6] In order to highlight the overall perspective, we invoke simple physical arguments in order to lend plausibility to the key results [Eqs. (2), (4), and (10)] of relevance to us. The case that we are going to make is for noninteracting (quasi)particles only, as is appropriate for the self-consistent single particle theories employed in standard quantum chemistry calculations.

Single reservoir. In the case of a single reservoir $\mathcal{R}$ with which the molecule exchanges (noninteracting) quasiparticles, one has

$$\Sigma^{<}(E) = if_{\mathcal{R}}(E)\Gamma(E). \tag{5}$$

We have denoted the anti-Hermitian piece of the self-energy, Eq. (1), by

$$\Gamma = -\frac{i}{2}(\Sigma - \Sigma^{\dagger}). \tag{6}$$

Crucially, it is assumed here that the reservoir (e.g., an electrode) is in a thermodynamic equilibrium, so that the occupation of its quasiparticle states is governed by the Fermi-Dirac distribution $f_{\mathcal{R}}(E)$.

Using Eqs. (1), (5), and (6), Eq. (4) can be rewritten as

$$n(\mathbf{x},\mathbf{x}') = \frac{i}{2\pi}\int dE f_{\mathcal{R}}(E)\ \langle \mathbf{x}|\mathcal{G}(\Sigma - \Sigma^{\dagger})\mathcal{G}^{\dagger}|\mathbf{x}'\rangle,$$

and with Eq. (1) one arrives at a well known fact,

$$n(\mathbf{x},\mathbf{x}') = -\frac{1}{\pi}\int dE f_{\mathcal{R}}(E)\ \langle \mathbf{x}|\mathrm{Im}\ \mathcal{G}|\mathbf{x}'\rangle. \tag{7}$$

Note that the occupation of states on the molecule is dictated by the Fermi distribution $f_{\mathcal{R}}$ of the reservoir. Roughly speaking, Eq. (7) expresses the density matrix as matrix elements of the "spectrally resolved density of states operator" summed over all states that are being filled from the reservoirs. In the absense of particle exchange,

$$-\frac{1}{\pi}\,\mathrm{Im}\,\mathcal{G} = \delta(E - H),$$

and one recovers the familiar expression (taking temperature to zero)

$$n(\mathbf{x},\mathbf{x}') = \sum_{p}^{\text{occ.}} \phi_p^*(\mathbf{x})\phi_p(\mathbf{x}') \tag{8}$$

in terms of the eigenstates ϕ_p of the single particle Hamiltonian H. This expression is employed in standard quantum chemistry and electronic structure codes.

Multiple reservoirs. The case of more than one reservoir, $\mathcal{R}_1, \mathcal{R}_2, \ldots$, owes its particular interest to the fact that, while each reservoir by itself may be in thermodynamic equilibrium, the combined system needs not to be. In other words, level occupation is still given by a Fermi-Dirac distribution, $f_{\mathcal{R}_r}$, but each reservoir is at its own (electron) temperature and chemical potential, μ_r.

The virtue of the Keldysh approach most important for us is that for noninteracting particles it can be easily generalized to this nonequilibrium situation. Namely, every reservoir $\mathcal{R}_r$ contributes with its own Σ_r to the broadening of the molecular energy levels,

$$\Sigma = \sum_r \Sigma_r, \tag{9}$$

independent of all the others. Also, the contribution to the density matrix made by every reservoir is simply additive

$$\Sigma^<(E) = i\sum_r f_{\mathcal{R}_r}(E)\Gamma_r(E). \tag{10}$$

The weight Γ_r of each electrode comes in very naturally here: imagine that a molecular level $|p\rangle$ is empty at $t=-\infty$, because at that early time the coupling of the molecule to the reservoirs is set to zero. Now, after switching on all couplings, electrons will gradually fill in the $|p\rangle$ level and each reservoir's share indeed is proportionate to its influx per time which is just Γ_r. This aspect is automatically taken care of in the formulation with $\Sigma^<$, Eq. (2), and for this reason it is so useful.

C. Model self-energies

In several instances, very useful approximate expressions for the self-energy Σ are available. We briefly discuss three important cases. We assume that the full Hamiltonian has been subject to partioning into a subsystem $\mathcal{M}$ ("molecule"), a reservoir $\mathcal{R}$, and a mutual coupling.

$$H = H_{\mathcal{M}} + H_{\mathcal{R}} + V. \tag{11}$$

(*a*) *Condensed matter electrode*. The coupling V is of the form

$$V = \sum_{m,k} v_{mk} d_m^\dagger c_k + \text{H.c.}, \tag{12}$$

where $d_m^\dagger, d_m$ denote the creation/annihilation operators in $\mathcal{M}$ Hilbert space and $c_k^\dagger, c_k$ the counterparts in $\mathcal{R}$ space. Then,[7]

$$\Sigma_{mm'}(t,t') = \sum_{kk'} v_{mk}\mathcal{G}_{\mathcal{R}}(k,k';t-t')v_{k'm'}. \tag{13}$$

v_{mk} describes the hopping from molecule to the electrode, $\mathcal{G}_{\mathcal{R}}$ represents the (unknown) dynamics of the reservoir, and $v_{k'm'}$ the hopping back to the molecule. In applications, we consider a Markovian approximation which is justified if a separation of time scales exists, as usual. In the present case, it is assumed that the time correlations between the two processes "electron leaving the molecule" and "electron reentering the molecule" decay on a time scale much faster than all other time scales characterizing the electron correlations on the molecule. In other words, we postulate that the absorption process itself must not provide an additional, relevant dynamics and hence keep only Σ diagonal elements in time space,

$$\Sigma(t,t') \approx \tilde{\Sigma}\delta(t-t'),$$

where

$$\tilde{\Sigma}_{mm'} = \sum_{kk'} v_{mk}\mathcal{G}_{\mathcal{R}}(k,k';E_F)v_{k'm'}. \tag{14}$$

The Markovian approximation is valid, roughly speaking, if the part of the lead included in the quantum chemistry calculation is large enough. In this case, the density of states of the lead material is already included in the space $\mathcal{M}$. If a slight smearing of the energy levels does not give the correct (smooth) density of states of the leads, this approximation cannot be used, in general.

Simplifying even further, reservoirs will be modeled later by modifying the spatial boundary conditions that the wave functions are subject to. Specifically, we employ absorbing boundary conditions that become active at the interface (or "surface," $\mathcal{S}$), where $\mathcal{M}$ couples to $\mathcal{R}$. In this model, the entries of $\tilde{\Sigma}$ are simply given by

$$\tilde{\Sigma}(\mathbf{x},\mathbf{x}') = (\delta\epsilon + i\eta)(\mathbf{x})\delta(\mathbf{x}-\mathbf{x}') \tag{15}$$

in real space representation. The local absorption rates $\eta(\mathbf{x})$ [and compensating energy shifts $\delta\epsilon(\mathbf{x})$] are allowed to take nonzero values only in the surface space $\mathcal{S}$. This drastic simplification has been introduced and tested for transport calculations in Ref. 8. The transmission curves thus obtained have been argued and explicitly demonstrated to be independent of the particular details of how $\eta(\mathbf{x})$ has been constructed. Practical choices of $\mathcal{S}$, $\eta(\mathbf{x})$, and $\delta\epsilon(\mathbf{x})$ are discussed in Sec. III.

For calculation of electron transport, one has to specify two different reservoirs (see Sec. III), but one can also imagine applications with one reservoir and the self-energy modeled in the above way: for investigations of processes on surfaces, the latter are sometimes modeled by finite clusters, e.g., the CO adsorption at a MgO surface.[9] Coupling the cluster to a reservoir simulating an infinite bulk could be a refinement here and might be a computationally cheap alternative to treatments with periodic boundary conditions.

(*b*) *Molecule in solution*. A molecule embedded in an electrochemical solution in principle is a much more complicated case, because in addition to the electronic degrees of freedom, also the motion of molecules in the background of other molecules should be taken into account. However, an important simplification arises if the concept of an "effective embedding medium" is applicable. In its simplest variant, the effective medium is homogenous. It is characterized by a

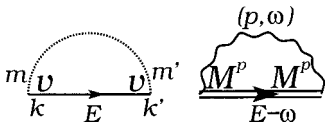

FIG. 1. Diagrammatic representation of self-energies. Left: propagation from the molecule (initial state m) into an electrode and back (final state m'), Eq. (13). Propagator inside electrode is denoted by a single solid line. Right: scattering of electrons at phonons (state p, frequency ω). Propagator on the molecule in the presence of electrodes, and phonons is denoted with a double solid line. For the definition of the vertex M^p and the phonon propagator (wiggly line), see Eqs. (17) and (21).

screening radius together with the level shift and broadening, $\epsilon_p + i\eta_p$, of each molecular eigenstate $|p\rangle$,

$$\tilde{\Sigma}_{pp'} = \delta_{p,p'}(\epsilon_p + i\eta_p). \tag{16}$$

The lifetime results from an exchange of electrons with the solution and is temperature dependent: $\sigma_p(T)$. Due to averaging, there is no spatial structure externally imposed. An explicit calculation of σ_p could start, for instance, from an analysis of ionization rates in low energy molecule-molecule scattering events. We do not pursue this topic here any further.

The screening radius accounts for the fact that the molecule is surrounded by a cloud of ionized molecules which carry the countercharge compensating for the molecular excess charge. The net charge of the combined system is exactly zero. In this situation, the screening provided by the cloud should also be taken into account. It can be modeled, for instance, by assuming that the counterions are located on a thin shell of a simple geometry surrounding the original molecule. The shell would act effectively as a metallic layer and could be incorporated by solving the Poisson equation under the constraint that the electrostatic potential on the shell is constant.[2]

(*d*) *Phonons and vibrons*. Emission and absorption of phonons can also be understood as an interaction between the fermions and the degrees of freedom of a bosonic bath. The exchange is in terms of energy, only, since the particle number is conserved. The interpretation of Σ is still a relaxation time, now due to de-/excitations of atomic vibrations.

We take the electron-phonon coupling of the form

$$V = \sum_p \sum_{m,m'} M^p_{mm'}(a_p^\dagger + a_p) d_m^\dagger d_{m'} \tag{17}$$

where $a_p^\dagger, a_p$ are creation and annihilation operators of phonons/vibrons with frequency ω_p and $M^p_{mm'}$ is the associated coupling matrix element.[10] In the case where the electron-phonon coupling is weak, it does not interfere with other relaxation mechanisms, so the relaxation rates are additive ("Mathiesen rule"[11]) and

$$\Sigma = \Sigma_{\mathcal{R}} + \Sigma_{\mathcal{V}}. \tag{18}$$

The phonon self-energy $\Sigma_{\mathcal{V}}$ has been defined in diagrammatic terms in Fig. 1.

Similarly, also the density matrix contains a term originating from scattering off vibrations, which again is additive so that

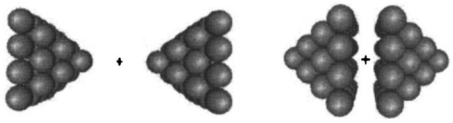

FIG. 2. Geometries used for test calculations. Left: tip-on-tip geometry; right: base-on-base geometry. Cross, "+," indicates location of the test charge.

$$\Sigma^< = \Sigma^<_{\mathcal{R}} + \Sigma^<_{\mathcal{V}}. \tag{19}$$

In the self-consistent Born approximation, one has

$$\mathbf{\Sigma}^<_{\mathcal{V}}(E) = i\sum_p \mathbf{M^p}\left[\int \frac{d\omega}{2\pi} D_p^<(\omega)\mathbf{\mathcal{G}}^<(E-\omega)\right]\mathbf{M^p}, \tag{20}$$

where a matrix notation has been introduced. Matrices acting on the molecular Hilbert space, $M^p_{mm'}$ and $\mathcal{G}^<_{mm'}$, are given in boldface capital letters. The propagator $D_p^<(\omega)$ describes the dynamics of the phonon in between the emission and reabsorption processes. In the simplest case, we can ignore the damping of the lattice vibrations due to the coupling to the fluctuating charge density. Then, $D_p(\omega)$ describes the propagation of free phonons, and we can write

$$D_p^<(\omega) = -2\pi i[(1+n_p)\delta(\omega+\omega_p) + n_p\delta(\omega-\omega_p)], \tag{21}$$

where n_p denotes the Bose function.[10]

III. IMPLEMENTATION FOR TRANSPORT CALCULATIONS BEYOND THE LINEAR RESPONSE

The implementation of reservoirs into the quantum chemistry code that we are working with, TURBOMOLE,[1,12] has been designed for determining the I/V characteristics. As we have pointed out already in Sec. II B, the important modification only concerns the computation of the density matrix.

A. Details of the calculation of $n(\mathbf{x},\mathbf{x}')$

We now give the details relevant in our implementation. Whenever the DFT self-consistency cycle (Sec. II A) calls for the construction of a new density matrix $n(\mathbf{x},\mathbf{x}')$, the program is stopped and the secondary process (see Scheme 1)

TABLE I. Leakage and shift parameters used in the construction of the model self-energy. First column: number of Au atoms included in a single (pyramid) electrode; in braces the number of Au atoms in the surface space $\mathcal{S}$ with nonzero leakage is also given. Atoms located in layers far remote from test charge location. Second column: distance (tip to tip or base to base) of electrodes. Third and fourth columns: parameters for model self-energy as defined in Eq. (15)

No. of Au (No. of Au with η)	Distance (a.u.) gold-gold	Leakage η (H)	Shift $\delta\epsilon$ (H)
14 (9)	8	0.03	0.02
14 (9)	18	0.1	0.07
18 (4)	9	0.1	0.063
18 (4)	19	0.1	0.07
30 (16)	10,20	0.1	0.065

Input:

- $\epsilon_p, c_{\nu p}$: eigenvalues and expansion coefficients of molecular orbitals $|p\rangle$ in basis $|\nu\rangle$
- $\eta_{L/R}, \delta\epsilon_{L/R}$: coupling parameters to left/right reservoir
- $\mu_{L/R}$: chemical potential of left/right reservoir

Calculation steps:

1. Calculate $S_{\nu\nu'}, S^{1/2}_{\nu\nu'}$ and orthogonalize molecular orbitals: $\tilde{c}_{\nu' p} = S^{1/2}_{\nu'\nu} c_{\nu p}$
2. Construct $H_{\nu'\nu} = \epsilon_p \tilde{c}_{\nu' p} \tilde{c}_{\nu p} + \Sigma_{\nu'\nu}$
$$\Sigma_{\nu'\nu} = \begin{cases} \delta_{\nu\nu'}(\delta\epsilon_{L/R} + i\eta_{L/R}) & \text{at coupling atoms} \\ 0 & \text{else} \end{cases}$$
3. Get eigenvalues Z_p and eigenvectors $b_{\kappa p}$ of $H_{\nu'\nu}$.
4. Calculate
$$\tilde{n}^{eq}_{\kappa\lambda} = b_{\kappa p}\left[1 + \tfrac{1}{2\pi}\left[\ln(\mu_L - Z^*_p) - \ln(\mu_L - Z_p)\right]\right] b_{p\lambda}$$
5. Form $b^{-1}_{p\nu}$,

   calculate $\tilde{N}_{pq} = b^{-1}_{p\nu} \Gamma^R_{\nu\nu'} b^{-1}_{\nu' q}$,
$$\Gamma^R_{\nu'\nu} = \begin{cases} \delta_{\nu'\nu}\eta_R & \text{at coupling atoms} \\ 0 & \text{else} \end{cases}$$
   then
$$\tilde{M}_{pq} = \frac{\tilde{N}_{pq}}{Z_p - Z^*_q}\ [\ \ln(\mu_R - Z^*_q) - \ln(\mu_R - Z_p) - \ln(\mu_L - Z^*_q) + \ln(\mu_L - Z_p)]$$
   and finally $\delta\tilde{n}_{\kappa\lambda} = \frac{1}{\pi} b_{\kappa p} \tilde{M}_{pq} b_{q\lambda}$.
6. Transform back: $n_{\nu\nu'} = S^{-1/2}_{\nu\kappa}\left[\tilde{n}^{eq}_{\kappa\lambda} + \delta\tilde{n}_{\kappa\lambda}\right] S^{-1/2}_{\lambda\nu'}$

is started in which $n(\mathbf{x},\mathbf{x}')$ is calculated. After the secondary process has finished, the primary resumes again, now taking the newly calculated density matrix. In the current (preliminary) implementation, the original module of the TURBOMOLE code[12] thus is nearly unmodified; calculation of the density matrix according to Scheme 1 is done by a separate program.

1. Green's function

Before we can start the matrix inversion, Eq. (1), that delivers $\mathcal{G}$, we need to specify the Hamiltonian and the self-energy.

Hamiltonian. The program provides in every iteration step updated Kohn-Sham (KS) orbitals $|p\rangle$ and (pseudo) energies ϵ_p. They can be used in order to construct the effective KS Hamiltonian,

$$H_{\mathcal{M}} = \sum_p \epsilon_p |p\rangle\langle p|. \tag{22}$$

The states $|p\rangle$ are given in a basis $|\mu\rangle$ of nonorthogonalized Gaussian functions. The wave function then is represented by the expansion coefficients $c_{\mu p}$. For convenience we convert to an orthogonal basis by a Loewdin orthonormalization, i.e., by transformation of the coefficients with the square root of the overlap matrix.

Self-energy. The self-energy that enters Green's function is approximated by the model of absorbing boundary conditions introduced in Ref. 8 and detailed in Eq. (15). This

model requires the specification of the surface space $\mathcal{S}$, which consists of the set of all atoms where absorption can occur (Sec. II C). In our model calculations, the electrodes take the form of tetragonal pyramids. If not specified otherwise, calculations are performed in the tip-on-tip geometry (see Fig. 2). The Au atoms of those layers, which are remote from the molecule, form the surface space $\mathcal{S}$.

Furthermore, the leakage function $\eta(\mathbf{x})$ needs to be constructed. We take η to be homogeneous on $\mathcal{S}$. The magnitude of η is a parameter, which has to be adjusted in such a way that the calculational results for physical observables do not change under variation of η. This condition is satisfied exactly in the limit of large electrodes. In practical calculations, the requirement always has to be explicitly checked. The energy shift $\delta\epsilon(\mathbf{x})$ was adjusted in such a way that the calculated Fermi level for the entire system takes the value of bulk Au. The combinations of values that we use in actual calculations are listed in Table I.

2. Density matrix

We employ Eq. (10) in order to obtain $\Sigma^<$. It is the key quantity entering in Eq. (4), which will ultimately deliver $n(\mathbf{x},\mathbf{x}')$. At this step a standard problem arises, which is to evaluate a spectral sum appearing in Eq. (4). The difficulty is that integral quantities like the density have contributions from all energies, not just from the vicinity of E_F, and therefore an integration of a matrix product over the entire energy range needs to be performed. A dramatic simplification arises, however, in the Markov limit, Eq. (14). Indeed, if the energy dependence of $\Sigma(E)$ is weak, or relevant only in a very narrow spectral range near E_F, then the spectral integral can be performed analytically and the evaluation of the density operator reduces to matrix multiplications.

We list the explicit expressions that we use. We begin with the decomposition of the density matrix as obtained by inserting Eq. (10) into Eq. (2) and the result in Eq. (4) for the special case of two reservoirs L and R with respective chemical potentials μ_L and μ_R.

$$n = \frac{1}{2\pi}\int_{-\infty}^{\mu_L} dE\mathcal{G}(\Gamma_L+\Gamma_R)\mathcal{G}^\dagger + \frac{1}{2\pi}\int_{\mu_L}^{\mu_R} dE\mathcal{G}\Gamma_R\mathcal{G}^\dagger, \quad (23)$$

$$= n_{\mathrm{eq}}(\mu_L) + \delta n. \quad (24)$$

In these expressions, we let $T=0$. Note that n is Hermitian and the particle density $n(\mathbf{x})=\langle\mathbf{x}|n|\mathbf{x}\rangle$ is real. In fact, also the off-diagonal elements are real, since $n=n^T$ so that $n=n^*$. To perform the integrations, we introduce eigenvalues Z_i and a matrix b, the columns of which denote the corresponding eigenvectors defined by

$$(H+\Sigma)b = bZ, \quad (25)$$

where $Z=\mathrm{diag}(Z_1,Z_2,\ldots)$. We also have

$$\mathcal{G}b = b(E-Z)^{-1}. \quad (26)$$

The first integral is trivially evaluated as

$$n_{\mathrm{eq}}(\mu_L) = b^\dagger b + \frac{1}{2\pi}[\ln(\mu_L - H - \Sigma^\dagger) - \ln(\mu_L - H - \Sigma)], \quad (27)$$

and after using the resolution of unity twice in the second term of Eq. (23), one obtains

$$\delta n = \frac{1}{2\pi} bMb^\dagger, \quad (28)$$

where the matrix elements of M are given by

$$M_{pq} = (b^{-1}\Gamma_R b^{\dagger-1})_{pq}\int_{\mu_L}^{\mu_R} dE \frac{1}{E-Z_p}\frac{1}{E-Z_q^*}. \quad (29)$$

Since our model coupling is energy independent, the eigenvalues Z_i do not depend on E. Therefore, the integral can be done analytically.

The resulting algorithm for the calculation of the density matrix n is sketched in Scheme 1. The most costly computational steps of the approach in its present formulation are two N^3 steps for the solution of the (complex) eigenvalue problem (step 3 in Scheme 1) in order to calculate b and the inversion of the complex matrix b (step 5).

B. Three simple tests

The algorithm was tested for systems shown in Figs. 2 and 6. Electrodes were modeled by Au clusters, usually of tetragonal pyramidal shape consisting of 3 or 4 layers (14 or 30 atoms). Additionally, we used an 18 atom cluster where the fourth layer consists of only 2×2 atoms. In a similar way a 71 atom cluster was obtained from a 5 layer pyramid with an additional 4×4 atom layer. The clusters are arranged either in tip-on-tip or in base-on-base position for various distances and oriented according to D_{2h} symmetry. Between them either point charges or a frequently used model system, 1,4-benzenedithiol (BDT), were placed, keeping the D_{2h} symmetry for consistency to various treatments (of other groups) presented in literature and for reasons of economy. Note, however, that for BDT in tip-on-tip position symmetry D_{2h} is not physical. Due to the presence of lone electron pairs at the sulfur atom, the correct C–S–Au angle is $\sim$110°; by the choice of D_{2h} symmetry it is enforced to 180°. (For further discussion see Sec. IV C.)

Calculations were carried out using the BP-86 functional,[13,14] basis sets of split-valence quality, def-SV(P),[15,16] and corresponding Coulomb-fitting basis sets;[16,17] relativistically corrected pseudopotentials covering the inner 60 electrons were used for Au.[18]

1. Charge neutrality and screening

In equilibrium, $\mu_L=\mu_R$, the entire system of molecule plus electrode pieces is charge neutral due to perfect screening—though partial charges on the molecule or near the junction may exist, of course. In our setup for the calculation of the density matrix, this charge neutrality is not *a priori* implemented, since we allow for the electron number N to fluctuate. Rather, at the end of the self-consistency

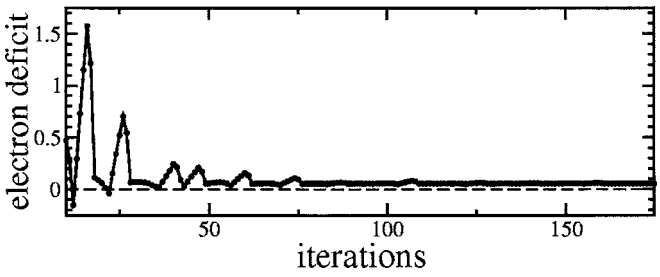

FIG. 3. Missing electrons (deviation from charge neutrality) at test charge $Q=0$ (Au_{18} tip on tip, $d=18$ a.u., $E_F=-5.05$).

cycle, N should have adjusted itself, so that it matches the number of positive charges in the system.

Whether or not our algorithm always satisfies charge neutrality, this is an important matter to test. To this end, we consider electrodes where the molecule has been replaced by a test charge Q (see Fig. 2). Q is only a vehicle to manipulate the overall charge in the system. It provides an electric potential, but it does not support electronic states, so electronic charge cannot accumulate at this point. A metal reacts to such a test charge with screening, i.e., additional charge $-Q$ flows in from infinity, and the subsystem of Q and the electrode pieces is charge neutral again. Ideally, our algorithm reproduces this behavior of Q.

In order to illustrate the convergence process, we have displayed in Fig. 3 how the total electron number changes from one iteration step to the next for a calculation at a system of type Au_{18}-Q-Au_{18} in tip-on-tip geometry. Indeed, at the point where the convergence has been reached, the deviation from charge neutrality is less than 5% of an electron and should decrease even more with increasing electrode size. The number of iterations is larger than in treatments with fixed particle number, as by releasing this constraint one more degree of freedom has to be optimized.

In Fig. 4 we display the charge Q' induced on the molecule, per test charge Q, as it is obtained for different geometries of the model electrodes (tip on tip, base on base, Fig. 2), different sizes (14, 18, or 30 gold atom pyramid), and separations. In all cases a point charge (without basis set) was placed in the center. The coupling $(\eta, \delta\epsilon)$ is shown in Table I. The ideal result would be the horizontal line with magnitude unity. The left panel shows results for the tip-on-tip position. A reasonably flat line close to value unity indeed is observed, if the distance of the electrode pieces is smaller than their typical spatial extension D (8 and 11 a.u.). On the other hand, also clear deviations of 15%–20% are seen, when this distance exceeds D (8 and 19 a.u.).

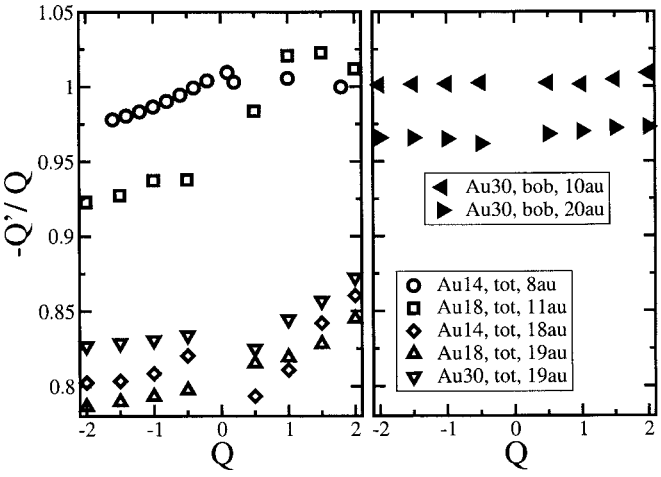

FIG. 4. Excess (or screening) charge Q' generated on the electrodes as response to an external test charge Q. Plotted is the ratio $-Q'/Q$ for different electrode models. Left: tip-on-tip (tot) geometry, three electrode sizes (Au_{14}, Au_{18}, Au_{30}), and for tot distances (8, 11, 18, and 19 a.u.). Right: Au_{30} in base-on-base (bob) arrangement at bob distances of 10 and 20 a.u.

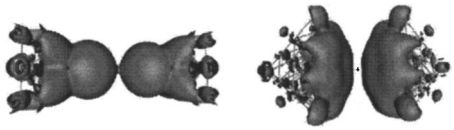

FIG. 5. Distribution of excess charge $Q=2|e|$ on Au_{14} electrode (left, distance tip-tip: 18 a.u.) and Au_{30} electrode (right, distance base-base: 18 a.u.).

This is not surprising. The effective screening area, where the compensating charge Q' would spread on a macroscopic electrode, grows with ever increasing distance of the test charge from the surface. We can only expect our model to describe those situations, in which this area is well confined to our model electrodes, i.e., at small separations of the pyramids and at values of Q not too large. In other words, the screening radius R_S must not increase beyond D.

Our reasoning suggests that for the purpose of modeling the screening process, the frequently used tip-on-tip geometry of pyramidal electrode pieces may be suboptimal. The pyramid geometry puts the screening electrode material relatively far away from the test charge (or molecule), so that the effective screening radius R_S is quite big (see Fig. 5, left panel). A geometric factor contained in R_S helps to suppress its magnitude. For example, if one chooses the base-on-base arrangement more screening charge can be deposited near the perturbation (see Fig. 5, right panel), and the charging ratio becomes very close to 1 (Fig. 4, right panel). Thus, we conclude that for suitable electrode geometry and distances not too large, screening is described very well by our algorithm.

2. Ground state charge density

Introducing the self-energy Σ modifies those properties of the combined system of electrodes and molecule, which are sensitive to the coupling of the surface region, $\mathcal{S}$. Obviously, the local density of states (DOS) in $\mathcal{S}$ is an example for such an observable sensitive in this sense. Ideally, the local DOS—and therefore the local electron density—would turn from a (111) Au surface into the bulk behavior upon switching on Σ. On the other hand, the particle density of the *molecule* is not susceptible to the surface region, if $\mathcal{S}$ is sufficiently far remote from the junction. It should be invariant under changes in Σ and, in particular, also under $\Sigma=i0$.

In order to test this expectation, the particle density for BDT has been determined for the setup shown in Fig. 6. In Fig. 7, upper panel, we show the line density $\rho(x)$ defined as the density $n(\mathbf{x})$ integrated over the transverse cross section

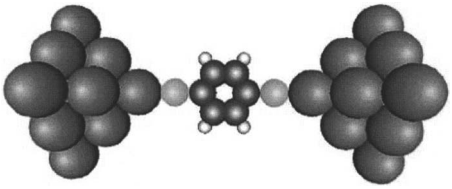

FIG. 6. Configuration of Au_{14}-BDT-Au_{14} used in model calculations ("symmetric coupling"). For details see text.

$$\rho(x) = \int dydzn(x;y,z).$$

Its pronounced structure is easily explained, since every peak represents a set of atoms that forms a transverse group. For a better resolution, Fig. 7 also has a lower panel that exhibits the difference in the charge densities $\rho_N - \rho_\mu$, as it is obtained with all boundaries facing vacuum (ρ_N, i.e., $\Sigma = i0$) against absorbing boundary conditions (ρ_μ). Deviations are strong in the region $\mathcal{S}$, in particular, in the base layer of Au atoms (9 Au, ±20 a.u.), but very small otherwise and negligible on the BDT molecule. The behavior is as expected.

The qualitative structure of the peaks near the base layer shows a relatively strong increase of charge inside the layer and the corresponding deficit in the vacuum region outside. The behavior is typical of a Au (111) surface. After cutting a Au crystal along the (111) direction, the approximately homogeneous density along the cutting plane of the bulk starts to relax and forms the "surface dipole." It is very important for the qualitative and quantitative understanding of a material's work function. In our model, these electronic relaxation processes that occur in the electrode pieces, after cutting them off from the macroscopic leads, are what Σ ultimately is supposed to revert, and, as suggested by Fig. 7, it really does.

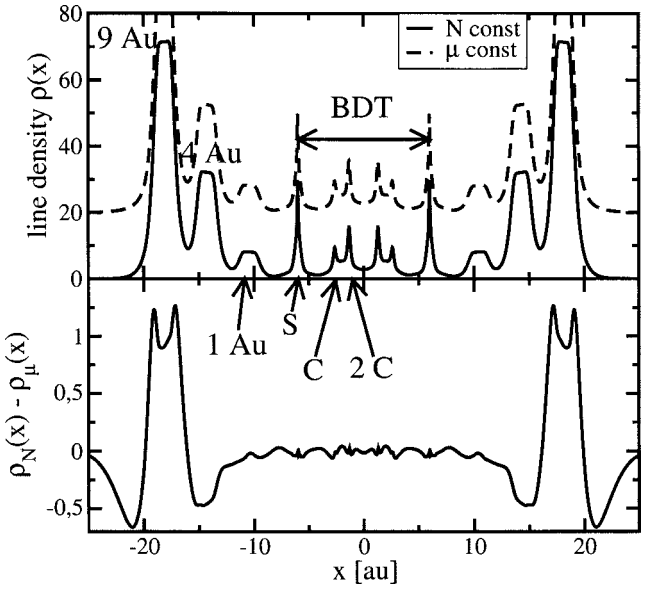

FIG. 7. Electron (line) density (sum over the transverse yz cross section) of Au_{14}-BDT-Au_{14}. Upper panel: calculations with fixed particle number (solid line) ρ_N and fixed chemical potential ρ_μ (dashed line, 20 offset y axis; $\mu = 5.032$ eV; 9 Au (remote layer) coupled, $\eta = 2$, 7 eV, $\delta\epsilon = 1.7$ eV). Lower panel: difference of line densities, $\rho_\mu - \rho_N$.

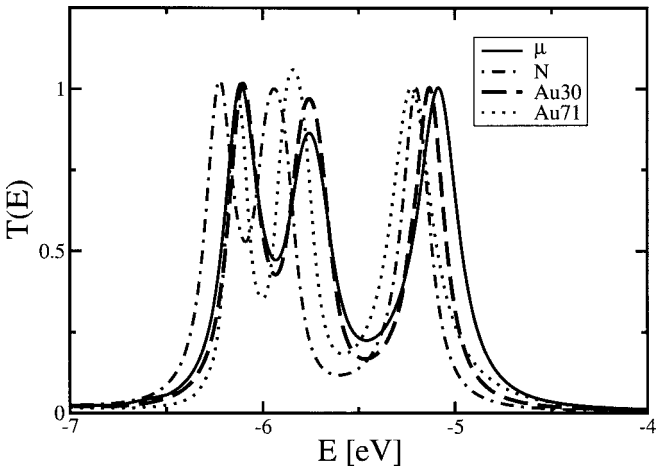

FIG. 8. Transmission of Au_n-BDT-Au_n for methods with fixed $N(n = 14, 30, 71)$ and fixed $\mu(n = 14)$. (In all calculations the last two layers are coupled with $\eta = 2.7$ eV.)

3. Transmission function

The particle density investigated in the previous section is a spectral integral and it tends to be much less amenable to surface effects than the spectral function itself that is summed over. In this section, we investigate the effect that Σ has on the molecular transmission characteristics, $T(E)$. It probes the spatial and spectral structures of individual Kohn-Sham orbitals, and therefore this quantity is much more sensitive to the details of modeling Σ than the overall particle density.

We will compare two different ways to calculate $T(E)$. The first calculation is not self-consistent: we perform a standard quantum chemistry calculation with fixed particle number, N (i.e., $\Sigma = i0$ in the iteration cycles). After convergence, we use the resulting effective single particle Hamiltonian H_N and construct from it Green's function [Eq. (2), now including Σ] and the transmission according to the Landauer formula

$$T(E) = \mathrm{tr}\, \Gamma_L \mathcal{G} \Gamma_R \mathcal{G}^\dagger, \tag{30}$$

where $\Gamma_{L,R}$ has already been defined below Eq. (5). The second procedure—our algorithm described in Sec. III—also employ Eq. (30), but it is self-consistent, because it uses an effective Hamiltonian H_μ (instead of H_N) that has been calculated already in the presence of electrodes. Clearly, in the macroscopic limit both procedures are equivalent. However, an important difference can exist in the way that this limit is approached. One suspects that convergence in the number of electrode atoms is faster for the self-consistent procedure.

In Fig. 8 the different transmission functions are shown, as obtained for the model system BDT, Fig. 6. Indeed, the positions of the transmitting orbitals with energies closest to E_F do not perfectly well coincide. As outlined above, the mismatch is not unexpected. Several mechanisms contribute. We only mention one: the effective electrode size felt by the KS orbitals is slightly different, depending on whether boundaries are absorbing or facing vacuum. Therefore, single particle states of electrodes can be shifted in energy and so can their hybrids with the molecular states.

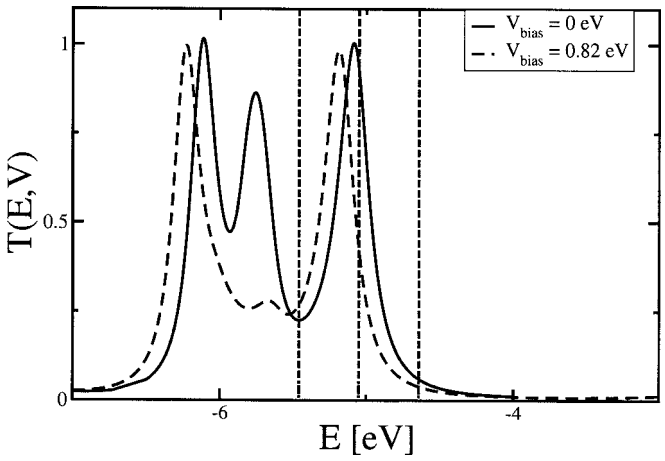

FIG. 9. Transmission function at zero (solid) and nonzero ($V_{\mathrm{bias}}=1.36$ eV, dashed) bias voltages. Center vertical line indicates E_F; neighboring vertical lines shows the voltage window for the dashed curve. Peaks in solid curve represent resonant transport through LUMO, HOMO/HOMO-1, and HOMO-2 of (free) benzene molecule. Due to bias voltage driven Stark effect, the center peaks "disappears;" only a small shoulder near ~5.7 eV remains. (Model system Au_{14}-BDT-Au_{14}, Fig. 6; self-energy, Eq. (15), with 9 atoms coupled for self-consistency loop and 13 atoms coupled for calculation of transmission; $\eta=0.1$ H, $\delta\epsilon=0.063$ H)

In order to see which one of the two procedures could be closer to the macroscopic limit, we also include in Fig. 8 results of a self-consistent calculation with the electrode size doubled once (Au_{30}) and twice (Au_{71}). Both of the smaller systems (Au_{14}) show peaks shifted as compared to the larger calculation, but the shifts among the self-consistent calculation are considerably smaller and convergence appears to be quite close.

IV. APPLICATION: NONLINEARITIES IN THE *I*/*V* CURVE OF BDT

In this section, we present an application of our formalism to the case of the BDT molecule (Fig. 6). Our aim is to calculate the I/V curve,

$$I=\int_{\mu_L}^{\mu_R} dET(E,V_{\mathrm{bias}}), \tag{31}$$

including effects on the transmission function, Eq. (30), that originate from the bias voltage, $V_{\mathrm{bias}}=\mu_R-\mu_L$.

A. Finite bias: Nonequilibrium Stark effects

Figure 9 shows the transmission function at two bias voltages, $V_{\mathrm{bias}}=0$ eV and $V_{\mathrm{bias}}=1.36$ eV. The overall trend imposed by the effects of finite bias is clearly visible: the transmission is suppressed.

On a qualitative level, a simple rational can be offered that explains the result of our DFT simulation. In the nonequilibrium situation KS orbitals and energies experience an effective electric field E_H. This field is produced mainly from the Hartree potential of the excess charges that populate either electrode.[42] The wave functions are calculated in the presence of this field, if $V_{\mathrm{bias}}\neq 0$, and therefore the transmission is voltage dependent.

For molecules with small level broadening, the effect of E_H can be understood qualitatively by considering a BDT molecule in a spatially homogenous, constant external electric field. The leading physics is subsumed in the Stark effect. For the readers' convenience we summarize the basic facts.

Since in our model geometry parity (under inversion along the S–S axis) is a good quantum number, electronic orbitals fall into two classes: (i) orbitals, for which symmetric and antisymmetric partners (even/odd parity) are nearly degenerate, and (ii) other orbitals, which are nondegenerate (but still show symmetry properties). Degenerate orbitals can be superposed into left- and right-centered states. The energy of such states moves linearly with increasing E_H, one state up and one down. By contrast, nondegenerate states have a vanishing dipole moment. They only show an effect to second order in E_H.

To illustrate these well known effects (and for later comparison with orbital deformation under a finite bias), we show in Fig. 10 how the highest occupied molecular orbital (HOMO) and neighboring orbitals of BDT are modified in an external electric field.

1. Nonequilibrium potential and level occupation

We will argue now that a very similar physics should also pertain to the case where the perturbing field is generated by a voltage drop between two reservoirs. Imagine first that the molecule is close to, but still uncoupled from, left and right electrodes. In that case our statement is trivial. Next, allow for a coupling and the corresponding current flow. Orbitals can populate now, or depopulate, and screening modifies the total electric field in the vicinity of the molecule. In this situation, one should distinguish orbitals that carry a current from those localized orbitals that do not. Localized orbitals still experience the conventional Stark effect, if in a modified total electric field.

By contrast, delocalized orbitals in principle need to be treated with more care. Imagine that the electrode-molecule coupling that we have introduced is tiny. In that case a simplification arises, because the full Hilbert space decouples into a piece that describes the molecule supporting $H^0_{\mathcal{M}}$, and the rest, which gives rise to some effective single particle potential, H',

$$H_{\mathcal{M}}=H^0_{\mathcal{M}}[n_{\mathcal{M}}]+H'(V_{\mathrm{bias}}),$$

together with a constraint. The constraint regulates the occupation of the eigenstates of $H_{\mathcal{M}}$ when calculating the density operator $n_{\mathcal{M}}$ of the molecule after coupling to the leads. It incorporates the fact that current carrying orbitals may only be partially filled. It renders $n_{\mathcal{M}}$ dependent on V_{bias}. Thus the constraint introduces an implicit bias dependency into $H_{\mathcal{M}}$ in addition to the explicit dependency contained in H'.

In certain cases, the implicit dependency of $H_{\mathcal{M}}$ on V_{bias} can be assumed small, because the filling of a current carrying orbital depends only weakly on the voltage. An example is that in the case of a level with symmetric, only weakly energy dependent couplings to both reservoirs, one always has a filling fraction of near 1/2. The dominating effect of a changing V_{bias} on the molecular orbitals is given by the po-

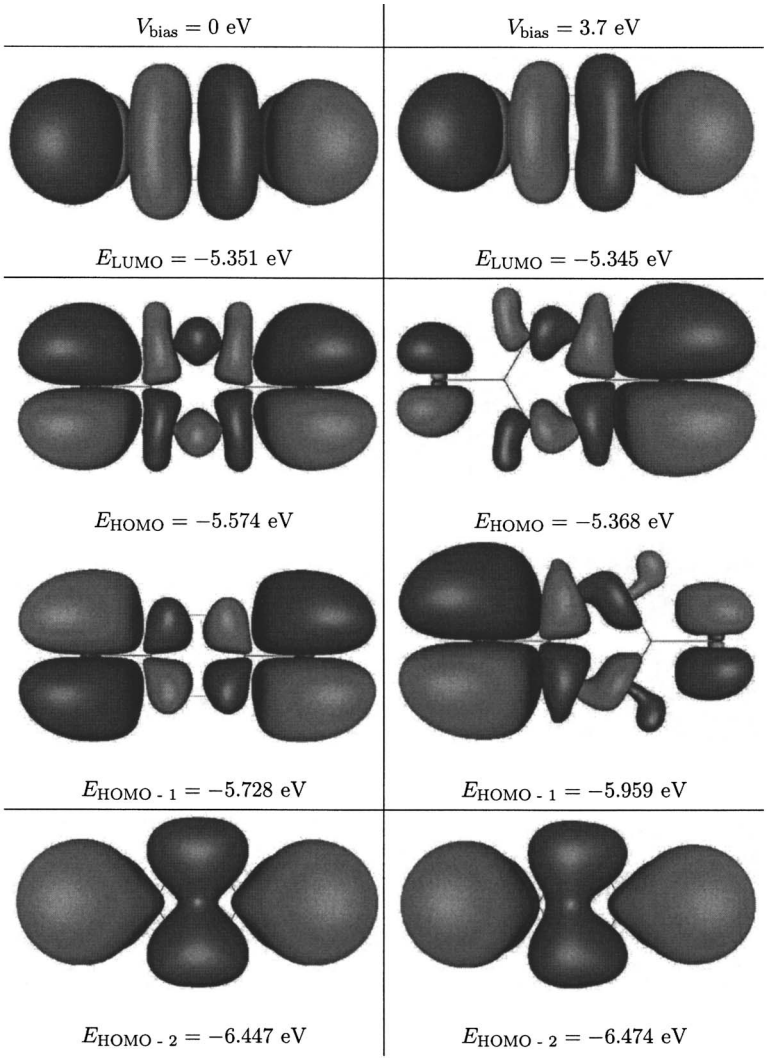

FIG. 10. Orbitals of BDT in vacuum and an electric field. Deformation of frontier orbitals of BDT driven by a static electric field (left: $E_{ex}=0$; right: $E_{ex}=0.01$ H/a.u.). Red and blue colors indicate positive and negative signs of the orbital wave function. LUMO and HOMO-2 are nondegenerate, exhibiting an effect of order E_{ex}^2. HOMO and HOMO-1 form an anti-/symmetric pair with energy splitting linear in E_{ex} and left/right localized split orbitals.

tential term $H'(V_{bias})$, as long as the (current driven) repopulation of the transport levels is very weak. In that case, the qualitative physics describing level deformation and levitation of conducting orbitals should remain just the one familiar from the conventional Stark effect.

2. Orbital transformation and levitation

We explain now how the Stark-type physics affects the conductance properties. Again, we first consider the case of two degenerate states localized left and right. Since a finite bias voltage lifts this degeneracy, the levels are driven out of their mutual resonance, i.e., they experience a voltage driven levitation. As a consequence, the current flow can be either through the left or through the right orbital, only, and since both of them are localized conduction is strongly suppressed.[43]

Similarly, in the nondegenerate case an orbital being (left-right) symmetric at zero bias transforms continuously. More and more orbital weight shifts away from regions with higher potential energy towards regions with lower potential energy, i.e., towards the electrode with the smaller chemical potential. Thus a "depletion" zone is generated, which is a molecular analog of a *p-n* junction.[19] Like in that familiar case, the overall current tends to decrease. Indeed, this expected behavior is in qualitative agreement with the observations made in Fig. 9.

Figure 11 shows the hybrid states that grow out of the orbitals shown in Fig. 10 after coupling to the electrodes. Comparing both figures, one can clearly see that similar deformations already seen for an isolated molecule also occur under a finite bias as expected.

B. Nonlinearities in the *I*/*V* curve

To illustrate the consequences of this orbital flow for transport, we first observe that the transmission curves, $T(E)$, Fig. 9, support three peaks. They indicate resonant tunneling through either a single or a degenerate pair of the orbitals displayed in Fig. 11. Specifically, the three peaks visible in $T(E)$ at $V_{bias}=0$ correspond to lowest unoccupied molecular orbital (LUMO), the pair HOMO/HOMO-1, and HOMO-2. Under a finite bias, $V_{bias}=1.36$ eV, the peaks produced by nondegenerate states remain largely unaffected, not so the degenerate levels, which split up and localize. Therefore, the degenerate peaks become very narrow and (due to the very asymmetric coupling of the left/right localized orbitals to the leads) the peak conductances also become very small. As a

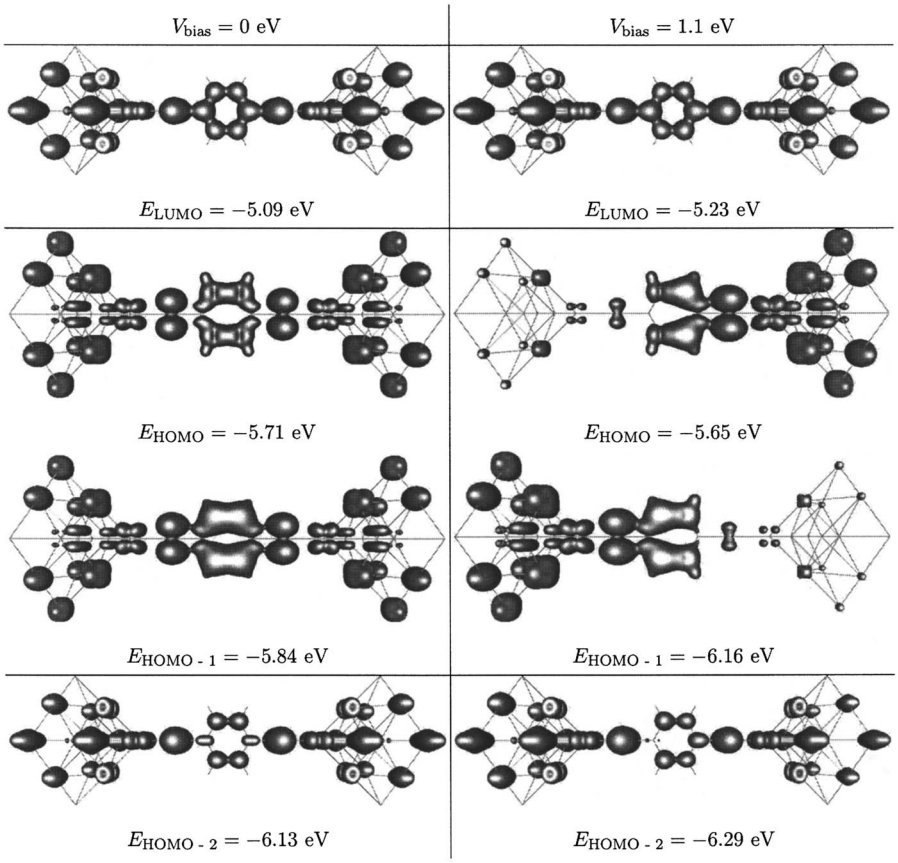

FIG. 11. Orbitals of BDT under applied bias voltage. Orbitals of BDT after coupling to the leads under zero (left) and finite (right) bias. Plot shows the absolute square of the same orbitals shown in Fig. 10. Comparing both figures, one sees that the level deformation associated with the Stark effect occurs in a similar way independent on whether or not a current is flowing. The general trend is that the Stark physics suppresses an orbital transmissivity.

consequence, the center peak essentially disappears, see Fig. 9. In other words, the nonequilibrium Stark effect renders the anti-symmetric pair a "dark state."

Next, we discuss the impact of the bias driven level flow on the I/V curve. Ignoring this flow, the dI/dV merely resembles the zero bias transmission. Figure 12 displays how deviations from this reference trace evolve with increasing bias voltage. In the particular case of BDT that we consider, the nonlinear effects tend to suppress the current and become strong if V_{bias} grows beyond ~1 eV. As already indicated above, we attribute current suppression mainly to the Stark pair HOMO/HOMO-1 falling dark. Note, however, that additional effects adding to current suppression exist. For instance, the peak indicating HOMO-2 flows down in energy, reaching −6.5 eV at a bias voltage V_{bias}=2.45 eV (not shown in the plots). Therefore, it drops outside the voltage window. This constitutes another mechanism for current suppression that is also active for symmetric orbitals and that is driven by the quadratic Stark effect.

C. Other theoretical works on BDT

Together with the alkanes, BDT has become the most commonly used test system for *ab initio* transport calculations. For this reason, many theoretical works mostly relying upon DFT (Refs. 4, 20–31, and 34) have been published;

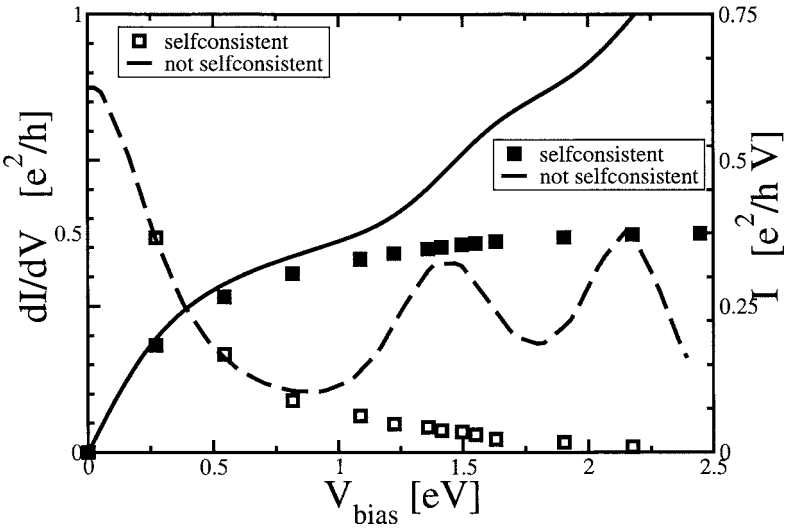

FIG. 12. I/V characteristics (solid line, filled □) and dI/dV (long dashed, open □) obtained from transmission curves calculated at various values of V_{bias} (two examples shown in Fig. 9) using Eq. (31). Also the corresponding traces ignoring the effect of V_{bias} on $T(E)$ are shown (solid lines). [Model system Au_{14}-BDT-Au_{14}, Fig. 6; self-energy, Eq. (15), with 9 atoms coupled for self-consistency loop and 13 atoms coupled for calculation of transmission; η=0.1 H, $\delta\epsilon$ =0.063 H.]

computations testing approaches advanced beyond DFT are available as well.[32,33] Providing a fair overview of this body of work is a challenging task. Even though most works employ the Landauer-Buttiker approach—like we do—detailed knowledge of implementation and procedure is absolutely necessary in order to understand the specific features of the computational results and the regime of validity. We shall refrain from such an endeavor, because it goes far beyond the scope of the present article. Instead, we will offer comments on a few basic issues.

Calculations differ by contact geometry, choice of functionals, implementation of (open) boundary conditions, transport fomalism, and most importantly in the extrapolation procedure into the macroscopic limit. The earliest full fledged DFT results for the BDT transmission, $T(E)$, at zero bias yielded smooth curves with very similar shapes.[4,22–24] The main difference is a certain shift in energy ($\lesssim 1$ V). Such shifts are not necessarily unphysical, since they indicate slight differences in the molecule-lead coupling. But also artifacts of modeling could be of relevance here, c.f. Sec. III B 3. *Cum grano salis* the earlier results have been confirmed by later authors; deviations in detail (fine substructures) persist.[27–29,31,34]

1. Sensitivity to contact geometry

The transmission is sensitive to the choice of contact geometry. Frequently used couplings are $S-Au_3$ ["hollow site" on plane (111) surface] and $S-Au_1$. The $S-Au_3$ coupling is stable under small variations of bond lengths and angles.[44] However, this is not true for every possible $S-Au_1$ coupling. For calculational speedup, often a "symmetric coupling," $S-Au_1^*$ is involved, with an angle of the Au–S–C bond of 180° (see Fig. 6), which imposes a spurious D_{2h} symmetry. This configuration is unstable, allowing the $S-Au_1^*$ geometry to relax (violating D_{2h} symmetry); the system moves into the $S-Au_1$ configuration with a physical angle close to 110°.[35]

In the artificial geometry $S-Au_1^*$, the transmission is not dramatically (i.e., by orders of magnitude) different from $S-Au_1$, if the coordination number of the bridging Au atom with other Au atoms is much larger than unity ("top site"). In this case, S orbitals overlap with orbitals of several Au atoms all contributing significantly to the level broadening. The main effects are that modified hybridization of molecular and lead orbitals (a) shifts the HOMO and other orbitals ($\lesssim 1$ eV) and (b) slightly decreases the overlap of resonances.

Important changes do occur when the coordination number of the bridging atom equals unity. In this case, the S atom sees just a single Au atom, and symmetry induced extinction of overlap matrix elements takes place. In this situation, the unphysical contact geometry $S-Au_1^*$ severely underestimates level broadening. It predicts that the zero bias conductance drops by one order of magnitude when an additional Au atom is attached.

We mention that a strong dependence of conductance on the length of the Au chain attached to the molecule has been reported in several theory publications.[20,27] Frequently it is argued that for this reason the effects of contacts on transport are overwhelming, so that the large discrepancies between theoretical calculations and experiments could be attributed to the unknown microscopic couplings, see, e.g., Ref. 20.

We would like to point out here that such an argument is clearly not valid, since the supporting calculations heavily rely on the use of the symmetric coupling. Its artificial character has been emphasized already by Bratkovsky and Kornilovitch.[21] Indeed, our calculations with the thermodynamically stable $S-Au_1$ geometry yield a transmission largely independent of the chain length.[35] This is the result that one actually would expect based on the fact that (a) N-atom Au wires ($N=2-4$) are perfect conductors[36] with (b) an I/V curve that is reasonably linear even at voltages $\lesssim 1$ V (Ref. 37), and (c) the $S-Au_1$ bonding is very strong.

2. Transmission and the Stark effect

While agreement about the shape of BDT's transmission at $V_{\mathrm{bias}}=0$ gradually seems to develop, important differences in the detailed changes of this curve when switching on V_{bias} persist. On a qualitative level, the general observation is that the overall transmission, $T(E,V_{\mathrm{bias}})$, appears to decrease with increasing V_{bias}.[23,24,30,31,38] To the best of our knowledge, a detailed explanation in terms of the Stark effect has not been given before.

The specific outreach of the Stark physics, which can be observed particularly well in the symmetric coupling, is the disappearance of the HOMO/HOMO-1 peak at larger voltages in Fig. 9. This phenomenon is nicely reproduced in the transmission curves, Fig. 6(c) of Ref. 31. However, the level flow as observed in several papers neither agrees with our simulation nor with the prediction made by the Stark effect. Namely, Refs. 31 and 38 seem to find *left-right symmetric*, nondegenerate orbitals to flow *linearly* in V_{bias} to higher energies. In these works a clear qualitative difference in the flow between symmetric (nonlocalized) and left or right localized orbitals does not appear, seemingly. It is hard to see how such a behavior could be reconciled with simple symmetry considerations. By contrast, we find a weak flow (indicative of V_{bias}^2 behavior) of symmetric orbitals and a linear flow of left/right localized states.

3. I/V curves

In general, comparing I/V curves is more difficult than transmission curves. Recall that a shift of $T(E)$ along the energy axis by 0.5 eV can easily occur, e.g., due to an uncertainty in the Fermi energy. It leaves the shape of $T(E)$ invariant and therefore cannot be considered an important qualitative difference. Nevertheless, such a shift can lead to drastic differences in I/V curves, the origin of which is not readily resolved unless the underlying transmission functions can be compared.

For this reason, I/V curves can easily look qualitatively different, while really the underlying evolution of the transmission function is very similar. We believe that this is the main reason for the large variability of I/V curves available even for the relatively simple test system of BDT. Let us emphasize, however, that despite of difficulties in reproducing the details mentioned already in the previous paragraph,

the plateau behavior in the I/V curve displayed in Fig. 12 that we explain in terms of the Stark effect has clearly been detected before by Stokbro *et al.*[22] and by Kondo *et al.*[31]

V. SUMMARY

In this work, a general methodology has been proposed and tested with the quantum chemistry code TURBOMOLE by which the effect of coupling reservoirs to a molecule can be studied. This coupling is facilitated by a model self-energy that effectively acts as an absorbing boundary condition for the self-consistent Kohn-Sham equations. As compared to an exact self-energy, our model has the advantage to speed up calculations at the expense of having to perform a systematic finite size analysis.

We have applied the method to study the nonlinearities in the I/V curve of BDT. We can show that simple but nontrivial physics like the Stark effect is properly incorporated in the procedure. This is important, because the bias induced deformation of orbitals can turn degenerate pairs of orbitals (left/right symmetric partners) into "dark states," which can have a substantial impact on the I/V characteristics, Fig. 9.

Very interesting situations could arise when the bias driven flow of orbital energies leads to a level crossing. In that case the molecule can undergo a substantial change in its electron (and also nuclei) configuration which can lead to a pronounced feature in the I/V curve. Also the qualitatives of such more complicated modifications can be studied within our framework.

We emphasize, however, that even though many qualitative aspects of transport through single molecules may be studied, great caution is required for extraction of quantitative information. Here, we have to restrict ourselves to a few basic remarks and refer the reader to the literature for details and recent developments.[39] The proposed approach has been implemented in an effective single particle formulation DFT, which is a theory for the ground state energy and particle density. As long as we stick to the calculation of these ground state characteristics, it is the approximation made in the exchange-correlation functional that limits the precision of the numerical results. However, when leaving the ground state sector and including excitations, as one does with a transport calculation, additional uncertainties appear. These are twofold. (a) The ground state functional ignores nonequilibrium corrections. (b) The self-energy $\Sigma^<$ may no longer be given by the simple form, Eq. (10). In particular, the level occupation is no longer guaranteed to be of the Fermi-Dirac type, appropriate for noninteracting particles. A thorough understanding under which conditions these effects give the dominating contributions to quantitative errors has not been achieved by now.

ACKNOWLEDGMENTS

The authors express their gratitude to A. Bagrets, V. Meded, D. Rappoport, and P. Wölfle for valuable discussions, as well as the DFG "Center for Functional Nanostructures" situated at Karlsruhe University for financial support. Also, they thank Sense Jan van der Molen for drawing their attention to Ref. 40. Moreover, their work as a whole has profitted from fruitful collaborations with K. Burke.

[1] R. Ahlrichs, M. Bär, M. Häser, H. Horn, and C. Kölmel, Chem. Phys. Lett. **162**, 165 (1989).
[2] A. Klamt, J. Phys. Chem. **99**, 2224 (1995).
[3] F. Evers, F. Weigend, and M. Koentopp, Physica E (Amsterdam) **18**, 255 (2003).
[4] F. Evers, F. Weigend, and M. Koentopp, Phys. Rev. B **69**, 235411 (2004).
[5] V. V. Maslyuk, A. Bagrets, V. Meded, A. Arnold, F. Evers, M. Brandbyge, T. Bredow, and I. Mertig, Phys. Rev. Lett. **97**, 097201 (2006).
[6] L. P. Kadanoff and G. Baym, *Quantum Statistical Mechanics* (Addison-Wesley, Reading, MA, 1962).
[7] Y. Meir and N. Wingreen, Phys. Rev. Lett. **68**, 2512 (1992).
[8] F. Evers and A. Arnold, e-print cond-mat/0611401; *CFN Lectures on Functional Nanostructures*, Springer Lecture Notes in Physics Vol. II (Springer Verlag Berlin, Heidelberg, New York).
[9] K. M. Neyman, P. S. Ruzankin, and N. Rösch, Chem. Phys. Lett. **246**, 564 (1995).
[10] G. Mahan, *Many Particle Physics* (Plenum, New York, 2000).
[11] N. Ashcroft and N. Mermin, *Solid State Physics*, International ed. (Saunders College, Philadelphia, 1976).
[12] TURBOMOLE V5-8; J. Chem. Phys. 98, 1372 (1993).
[13] A. Becke, J. Chem. Phys. **98**, 1372 (1993).
[14] J. Perdew, Phys. Rev. B **33**, 8822 (1986).
[15] A. Schäfer, H. Horn, and R. Ahlrichs, J. Chem. Phys. **97**, 2571 (1992).
[16] K. Eichkorn, F. Weigend, O. Treutler, and R. Ahlrichs, Theor. Chem. Acc. **97**, 119 (1997).
[17] K. Eichkorn, O. Treutler, and H. Öhm, Chem. Phys. Lett. **240**, 283 (1995).
[18] D. Andrae, U. Häussermann, M. Dolg, H. Stoll, and H. Preuss, Theor. Chim. Acta **77**, 123 (1990).
[19] M. Elbing, R. Ochs, M. Koentopp, M. Fischer, C. von Hänisch, F. Weigend, F. Evers, H. B. Weber, and M. Mayor, Proc. Natl. Acad. Sci. U.S.A. **102**, 8815 (2005).
[20] M. Di Ventra, S. Pantelides, and N. Lang, Phys. Rev. Lett. **84**, 979 (2000).
[21] A. M. Bratkovsky and P. E. Kornilovitch, Phys. Rev. B **67**, 115307 (2003).
[22] K. Stokbro, J. Taylor, M. Brandbyge, J.-L. Mozos, and P. Ordejon, Comput. Mater. Sci. **27**, 151 (2003).
[23] Y. Xue and M. A. Ratner, Phys. Rev. B **68**, 115406 (2003).
[24] S. V. Faleev, F. Leonard, D. A. Stewart, and M. van Schilfgaarde, Phys. Rev. B **71**, 195422 (2005).
[25] G. C. Solomon, J. R. Reimers, and N. S. Hush, J. Chem. Phys. **121**, 6615 (2004).
[26] S.-H. Ke, H. U. Baranger, and W. Yang, J. Chem. Phys. **122**, 074704 (2005).
[27] S.-H. Ke, H. U. Baranger, and W. Yang, J. Chem. Phys. **123**, 114701 (2005).
[28] K. S. Thygesen and K. W. Jacobsen, Chem. Phys. **319**, 111 (2005).
[29] V. M. Garcia-Suarez, T. Kostyrko, S. Bailey, C. Lambert, and B. R. Bulka, e-print cond-mat/0610321v1.
[30] A. Grigoriev, J. Skoldberg, G. Wendin, and Z. Crljen, Phys. Rev. B **74**, 045401 (2006).
[31] H. Kondo, H. Kino, J. Nara, T. Ozaki, and T. Ohno, Phys. Rev. B **73**, 235323 (2006).
[32] P. Delaney and J. C. Greer, Phys. Rev. Lett. **93**, 036805 (2004).
[33] C. Toher, A. Filippetti, S. Sanvito, and K. Burke, Phys. Rev. Lett. **95**, 146402 (2005).
[34] G. C. Solomon, A. Gagliardi, A. Pecchia, T. Frauenheim, A. D. Carlo, J. R. Reimers, and N. S. Hush, Nano Lett. **6**, 2431 (2006).
[35] A. Arnold, M. Koentopp, and F. Evers (unpublished).
[36] N. Agrait, A. L. Yeyati, and J. M. van Ruitenbeek, Phys. Rep. **377**, 81 (2003).
[37] K. Hansen, S. Nielsen, M. Brandbyge, E. Lægsgaard, I. Stensgaard, and F. Besenbacher, Appl. Phys. Lett. **77**, 708 (2000).
[38] K. Stokbro (unpublished); data reproduced in Ref. 29.
[39] F. Evers and K. Burke, *CRC Handbook on Molecular Electronics*, edited by S. Lyshevsky (CRC, Boca Raton, FL, in press).
[40] M. Yu, N. Bovet, C. J. Satterley, S. Bengio, K. R. J. Lovelock, P. K. Milligan, R. G. Jones, D. P. Woodruff, and V. Dhanak, Phys. Rev. Lett. **97**, 166102 (2006).
[41] M. Brandbyge, J.-L. Mozos, P. Ordejon, J. Taylor, and K. Stokbro, Phys.

Rev. B **65**, 165401 (2002).

[42] Note that our setup realizes the bias voltage by charging electrodes similar to a battery. The difference in electrochemical potentials, $V_{\mathrm{bias}}=\mu_L-\mu_R$, stems from an inhomogeneity in the carrier density. Therefore, an externally applied potential ϕ_{ex} does not appear in the formalism. This is a technical simplification as compared to other realizations, where electrodes are uncharged. There one needs to introduce ϕ_{ex} in order to generate V_{bias} (Ref. 41).

[43] This voltage induced current suppression can lead to a negative differential conductance (NDR), if one of the degenerate levels should reside at the Fermi energy. Under this condition, the conductance is large at very small voltages below the level broadening, $V \ll \Gamma$, but it becomes very small as soon as V exceeds the level splitting, so that the states become left/right localized. Indeed, in Ref. 26 authors report NDR for BDT at voltages between 0.2 and 0.5 eV. However, the (nearly) degenerate pair HOMO/HOMO-1 have energies ~0.6 eV below E_F and we cannot confirm NDR, see Fig. 12; instead we observe that the transmission function $T(E)$ as calculated in Ref. 26 exhibits very sharp features on scales below 0.1 eV. The physical origin of such a spiky behavior remains unclear to us and perhaps it is related to the reported NDR. Smooth transmission curves $T(E)$ in a subsequent publication (Ref. 27) of the same group match our results reasonably well.

[44] This statement is correct only on planar surfaces. In the vicinity of edges, $\mathrm{S-Au_3}$ loses stability and a $\mathrm{S-Au_2}$ or $\mathrm{S-Au_1}$ coupling are preferable (Ref. 4). Recent experimental results for adsorbtion of thiols on Au (111) with Au adatoms are in support of these results (Ref. 40).